


Computational analysis of induced magnetohydrodynamic non-Newtonian nanofluid flow over nonlinear stretching sheet

Progress in Reaction Kinetics and Mechanism
Volume 47: 1–18
© The Author(s) 2022
Article reuse guidelines:
sagepub.com/journals-permissions
DOI: 10.1177/14686783211072712
journals.sagepub.com/home/prk


Muhammad Imran Anwar¹, Hina Firdous², A.Al Zubaidi³,
Nadeem Abbas⁴ and Sohail Nadeem⁵

Abstract

In the current article, induced magnetic field applied on second-grade fluid flow under variable thermal conductivity by an exponentially stretching sheet is taken into account for current analysis. The chemical reaction and viscous dissipation effects under the influence of thermophoresis and Brownian motion are considered on an exponentially stretching sheet. With the above assumptions, a mathematical model was developed in terms of partial differential equations by using the boundary-layer approximations. Similarity transformations in terms of ordinary differential equations considerably simplified this system. The dimensionless system was solved by a numerical procedure, the bvp4c method. The effects of involving physical parameters are presented through graphs and tables. The obtained numerical outcomes of the skin friction coefficient, the Sherwood number, and the Nusselt number are also highlighted in the tabulated form. It is concluded that the velocity and concentration profiles increased due to higher values of material parameter.

Keywords

Second-grade nanofluid, induced magnetic field, variable thermal conductivity, exponentially stretching sheet

¹Department of Mathematics, Higher Education Department, Punjab, Lahore, Pakistan

²Department of Sciences and Humanities, National University of Computer and Emerging Sciences, Lahore Campus, Pakistan

³Department of Mathematics, College of Science, King Khalid University, Abha, Saudi Arabia

⁴Department of Mathematics, Riphah International University Faisalabad Campus, Pakistan

⁵Department of Mathematics, Quaid-i-Azam University, Islamabad, Pakistan

Corresponding author:

Nadeem Abbas, Riphah International University Faisalabad Campus, Faisalabad, Pakistan.

E-mail: nadeem.abbas@riphahfsd.edu.pk



Creative Commons Non Commercial CC BY-NC: This article is distributed under the terms of the Creative Commons Attribution-NonCommercial 4.0 License (<https://creativecommons.org/licenses/by-nc/4.0/>) which permits non-commercial use, reproduction and distribution of the work without further permission provided the original work is attributed as specified on the SAGE and Open Access pages (<https://us.sagepub.com/en-us/nam/open-access-at-sage>).

Introduction

The MHD fluid flow has many applications namely: petroleum, warming system, electrostatic mechanism, power generation, modern metallurgy, pumping having the essential role in usual life. Damesh¹ discussed the thermal boundary layer in the existence of a magnetic field's impact by virtue of an exponentially stretching surface. Ishak² considered the MHD flow of a fluid having a linear radiative effect on an exponentially stretching surface. The unsteady two-dimensional boundary-layer flow of an incompressible Newtonian fluid under the thermal reaction, magnetic field, and absorption/heat generation impacts by virtue of an exponentially stretched surface was discussed by Elbashebeshy et al.³ Nadeem et al.⁴ discussed the MHD flow of a Casson fluid by an exponentially shrunk surface. Ferdows et al.⁵ presented the numerical solutions for the flow of fluid having nanoparticles due to the effect of MHD across a porous medium by virtue of a vertical exponentially stretching sheet. Impacts of chemical reaction for MHD flow of third-grade liquid by an exponentially stretching surface are discussed by Hayat et al.⁶ In the recent period, a few investigators worked on the MHD flow concept under various assumptions (see Refs. 7-10).

Initially, the idea of the flow of fluid by an exponentially stretched sheet was given by Magyari and Keller.¹¹ They discussed the numerical solutions for the fluid flow toward an exponentially stretched surface, and distributed the fact of mass and heat transfer properties. The idea of the fluid flowing toward an exponentially stretched sheet plays a vital factor in industries and engineering fields such as glass fiber, drilling of sheets and plastic films, paper production, annealing and thinning of the copper wire, etc. It is worth mentioning that the stretched velocity is not linear in all the conditions, so the stretched velocity of the fluid may be nonlinear or exponentially stretching. The flow of Newtonian and non-Newtonian fluid by virtue of an exponentially stretched surface has been discussed by scientists in the recent past. Partha et al.¹² considered an exponentially vertical surface to study the heat transportation with thermal mixed convection flow under the significance of viscous dissipation. Pal¹³ provided numerical solutions, and analysis follows to narrate the mixed convection flow by considering a vertical exponential surface with an exponentially dependent stretching velocity. The MHD, velocity, and the thermal slip effects were used by Mukhopadhyay,¹⁴ who analyzed the heat and mass transportation by a porous exponentially stretched surface with suction or blowing. Also, Mukhopadhyay¹⁵ utilized a thermally stratified medium and made numerical solutions for the magnetohydrodynamic flow by virtue of an exponentially stretched surface. Hussain et al.¹⁶ deliberated the two-dimensional MHD flow of second-grade liquid with nanoparticles by virtue of the exponentially stretched surface. Beg et al.¹⁷ discussed the effects of unsteady MHD nanofluid flow over a vertical exponentially stretching sheet. Veerasha et al.¹⁸ surveyed the heat and mass transportation impact in a boundary-layer MHD flow of viscous fluid into a permeable medium by virtue of an exponentially stretched surface. Several authors discuss the different problems of the boundary-layer flow using different models to analyze the behavior of heat transfer and its effects (see Refs. 19-21).

A fluid in which nanoparticles are submerged is called nanofluid. The size of nanoparticles is from 1 nm to 100 nm. The thermal conductivity of the nanofluids as compared to the base fluid is higher. Hence, nanofluids are the best source to raise the thermal conductivity to the base fluid. By virtue of such important features, the nanofluids are used in many fields of life such as heat exchanger vehicle cooling, nuclear reactors, biomedicine transfer cooling, electronic devices, etc. The magnetic nanofluids are used in MHD power generators, hyperthermia, removal of blockage in the arteries, in cancer therapy, treatment of cancer tumors, etc. Choi²² was the first scientist who used the term nanofluid. Pop and Khan²³ numerically discussed the flow of the fluid with nanoparticles under the impacts of thermophoresis and Brownian motion over a stretching surface. Makinde and

Aziz²⁴ analyzed the nanofluid behavior of the laminar boundary-layer flow with the impact of convective boundary condition on a stretched sheet. Rana and Bhargava²⁵ numerically performed and discussed the laminar boundary fluid flow under the effect of nanoparticles through a nonlinear stretching sheet. Hady et al.²⁶ considered a viscous nanofluid flow and numerically examined the heat transportation with the significance of nonlinear thermal radiation and variable wall temperature toward a nonlinear stretched sheet. Rashdi et al.²⁷ used nanofluid with the thermal and buoyancy radiation's influence on the magnetohydrodynamic flow toward a stretched surface. Greasha et al.²⁸ characterized the inspiration of heat absorption or generation and nonlinear thermal radiation with a porous medium for the three-dimensional flow of Jeffery nanofluid by a nonlinear porous stretching sheet. Several authors investigated the effects of flow behavior with diffusion with COVID-19 (see Refs. 29-33).

In the recent work, we examined the MHD flow of second-grade nanofluid with the existence of induced magnetic field, thermophoretic effect, variable chemical reaction, and variable thermal conductivity. By employing the similarity transformation, the governing boundary-layer PDEs changed into the nonlinear ODEs, and they were numerically solved by the built-in `bvp4c` technique. The effect of different dimensionless parameters on the induced magnetic field profile, temperature profile, velocity profile, and concentration profile are debated graphically. Further, the skin friction, Sherwood number, and Nusselt number are calculated and discussed. These results are more advanced and may be useful in industrial and engineering problems.

Mathematical formulation

Consider an incompressible, steady 2D of MHD second-grade fluid flow with the consequences of viscous dissipation, induced magnetic field, variable chemical reaction, and thermophoretic effect. The flow of the fluid is along the x -axis. The flow of the fluid is considered by virtue of an exponentially stretched sheet with the velocity $u_w = U_0 e^{x/l}$. The description of the coordinates and the physical chart are given in Figure 1.

By using the upper suppositions, the boundary-layer equations are

$$\frac{\partial u}{\partial x} + \frac{\partial v}{\partial y} = 0 \quad (1)$$

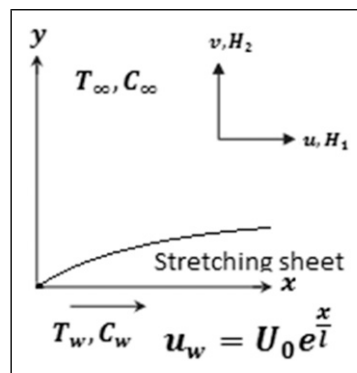


Figure 1. Coordinates and the physical chart.

$$\frac{\partial H_1}{\partial x} + \frac{\partial H_2}{\partial y} = 0, \quad (2)$$

$$u \frac{\partial u}{\partial x} + v \frac{\partial u}{\partial y} = v \frac{\partial^2 u}{\partial y^2} + \frac{\alpha_1}{\rho} \left[\frac{\partial}{\partial x} \left(u \frac{\partial^2 u}{\partial y^2} \right) + \frac{\partial u}{\partial y} \frac{\partial^2 u}{\partial x \partial y} + v \frac{\partial^3 u}{\partial y^3} \right] + \frac{\mu_0}{4\pi\rho_f} \left[H_1 \frac{\partial H_1}{\partial x} + H_2 \frac{\partial H_1}{\partial y} \right], \quad (3)$$

$$u \frac{\partial H_1}{\partial x} + v \frac{\partial H_1}{\partial y} = \alpha_2 \frac{\partial^2 H_1}{\partial y^2} + H_1 \frac{\partial u}{\partial x} + H_2 \frac{\partial u}{\partial y}, \quad (4)$$

$$u \frac{\partial T}{\partial x} + v \frac{\partial T}{\partial y} = \frac{1}{\rho C_p} \frac{\partial}{\partial y} \left[k(T) \frac{\partial T}{\partial y} \right] + \left[\frac{D_B \frac{\partial C}{\partial y} \frac{\partial T}{\partial y}}{+ \frac{D_T}{T_\infty} \left(\frac{\partial T}{\partial y} \right)^2} \right] + \frac{\mu}{\rho C_p} \left(\frac{\partial u}{\partial y} \right)^2 + \frac{\alpha_1}{\rho C_p} \frac{\partial u}{\partial y} \left[\frac{\partial}{\partial y} \left(u \frac{\partial u}{\partial x} + v \frac{\partial u}{\partial y} \right) \right], \quad (5)$$

$$u \frac{\partial C}{\partial x} + v \frac{\partial C}{\partial y} = D_B \frac{\partial^2 C}{\partial y^2} + \frac{D_T}{T_\infty} \left(\frac{\partial^2 T}{\partial y^2} \right) - \frac{\partial}{\partial y} (V_T C). \quad (6)$$

Here $k(T)$ and V_T are defined as

$$k(T) = k_\infty \left(1 + \varepsilon \frac{T - T_\infty}{\Delta T} \right), \quad V_T = -v_i \frac{k_1^*}{T_r} \frac{\partial T}{\partial y},$$

Here, ρ , v , k , μ_0 , α_1 , α_2 , H_1 , H_2 , C_p , D_B , D_T , T_∞ , μ , k_∞ , ε , V_T , and C_1 are the fluid density, kinematic viscosity, thermal conductivity, magnetic permeability, second-grade parameter, magnetic diffusivity of the nanofluid, component of the induced magnetic field along the x-axis, component of the induced magnetic field component along the y-axis, the heat capacity, coefficient of Brownian motion, thermophoresis coefficient, ambient temperature, fluid dynamic viscosity, fluid viscosity, fluid thermal conductivity, small parameter, and chemical reaction coefficient, respectively. The boundary conditions are

$$\begin{aligned} u = u_w = U_0 e^{\lambda y}, \quad v = 0, \quad H_1 = 0, \quad \frac{\partial H_1}{\partial y} = H_2 = 0, \quad C = C_w + \lambda_2 \frac{\partial C}{\partial y}, \\ T = T_w + \lambda_1 \frac{\partial T}{\partial y} \text{ at } y \rightarrow 0, \\ u \rightarrow 0, \quad H_1 \rightarrow H_\infty, \quad T \rightarrow T_\infty, \quad C \rightarrow C_\infty \text{ at } y \rightarrow \infty. \end{aligned} \quad (7)$$

Here, $H_\infty = H_0 e^{\lambda l}$.

Following are the similarity transformations

$$\begin{aligned}
 u &= U_0 \exp\left(\frac{x}{l}\right) f'(\eta), \quad v = -\sqrt{\frac{\nu U_0}{2l}} \exp\left(\frac{x}{2l}\right) [f(\eta) + \eta f'(\eta)], \quad \eta = \sqrt{\frac{U_0}{2\nu l}} \exp\left(\frac{x}{2l}\right) y, \\
 T &= T_\infty + T_0 \exp\left(\frac{x}{2l}\right) \theta(\eta), \quad C = C_\infty + C_0 \exp\left(\frac{x}{2l}\right) \varphi(\eta), \quad H_1 = H_0 \exp\left(\frac{x}{l}\right) h'(\eta), \\
 H_2 &= -\sqrt{\frac{\nu}{U_0 2l}} H_0 \exp\left(\frac{x}{2l}\right) (h(\eta) + \eta h'(\eta))
 \end{aligned} \tag{8}$$

After using the above similarity transformations (8), the PDEs (3)–(6) are transformed into the following ODEs (9)–(12)

$$2f'^2 - f f'' = f''' + A \left[3f' f''' + \eta f'' f''' - \frac{1}{2} f f^{iv} \right] + M \left[2h'^2 - h h'' \right], \frac{n!}{r!(n-r)!} \tag{9}$$

$$h''' = P_{rm} [h f'' - f h''], \tag{10}$$

$$P_r (f' \theta - f \theta') = (1 + \varepsilon \theta) \theta'' + \varepsilon \theta^2 + P_r (N_b \theta' \varphi' + N_t \theta^2) + P_r E_c [f''^2 + M f'^2 + A f'' (f' f'' - f f''')], \tag{11}$$

$$f' \varphi - f \varphi' = \frac{1}{S_c} \varphi'' + \frac{N_t}{S_c N_b} \theta'' - \tau_1 (\theta' \varphi' - (\theta + C_1) \theta''), \tag{12}$$

The corresponding boundary conditions are as follows

$$\begin{aligned}
 f &= 0, \quad f' = 1, \quad h = 0, \quad h' = 0, \quad \theta = 1 + S_1 \theta', \quad \varphi = 1 + S_2 \varphi', \quad \text{at } \eta \rightarrow 0 \\
 f' &= 0, \quad h' = 1, \quad \varphi = 0, \quad \theta = 0, \quad \text{at } \eta \rightarrow \infty.
 \end{aligned} \tag{13}$$

$A = \alpha_1 / \rho U_0 / \nu l e^{x/l}$ (second-grade parameter), $M = \mu / 4\pi\rho H_0^2 / U_0^2$ (magnetic field parameter), $P_r = \nu / \alpha_1$ (Prandtl number), $P_{rm} = \nu / \eta$ (magnetic Prandtl number), $N_b = D_B C_0 / \nu e^{x/2l}$ (parameter of Brownian motion), $N_t = D_T T_0 / \nu T_\infty e^{x/2l}$ (thermophoresis effect parameter), $S_c = \nu / D_B$ (Smith number), $\tau_1 = -k^*(T_w - T_\infty) / T_r$ (thermophoretic effect parameter), and $C_1 = (C_w - C_\infty) / C_\infty$ (concentration difference parameter).

The expressions of the physical quantities of interests like skin friction, Nusselt number, and Sherwood number are defined as

$$\begin{aligned}
 C_{fx} &= \frac{\tau_w}{\frac{1}{2} \rho u_w^2}, \\
 \tau_w &= \left[\mu \frac{\partial u}{\partial y} + \rho \alpha_1 \left(2 \frac{\partial u}{\partial x} \frac{\partial u}{\partial y} + u \frac{\partial^2 u}{\partial x \partial y} \right) \right]_{y=0}, \\
 C_{fx|\eta=0} &= \left(\frac{R_e}{2} \right)^{-\frac{1}{2}} [1 + 3\alpha f'(0)] f''(0),
 \end{aligned}$$

$$N_{ux} = \frac{xq_w}{k(T - T_\infty)},$$

$$q_w = \left| -k \left(\frac{\partial T}{\partial y} \right) \right|_{y=0}$$

$$R_e^{-\frac{1}{2}} N_{ux} = -\theta'(0),$$

$$Sh_x = \frac{xh_m}{D_B(\varphi_w - \varphi_\infty)}$$

$$S_{hx} = -\frac{x}{(C_w - C_\infty)} \left(\frac{\partial C}{\partial y} \right) \Big|_{y=0}, S_{hx} = -\sqrt{\frac{x}{l}} \left(\frac{R_{ex}}{2} \right)^{-\frac{1}{2}} \varphi'(0), S_{hx} \sqrt{\frac{2l}{x}} (R_{ex})^{-\frac{1}{2}} = -\varphi'(0).$$

Results and discussion

The second-grade fluid flow analysis of induced magnetic flow over an exponentially stretching sheet is taken into account. The model is developed under flow assumptions, and solved through a numerical technique. The graphical results are observed and effects are highlighted in Figures 2–15. Figure 2 presented the variation of A and $f'(\eta)$. It is prominent that $f'(\eta)$ declined due to higher values of A . It means that thickness of the boundary layer reduced for higher values of the material parameter because the stress applied resists strain and shear flow linearly. These phenomena reduce the velocity profile because the thickness of the fluid is enhanced. Figure 3 displays the variation of $f'(\eta)$ with M . The thickness of the velocity function declined due to enhancing the values of M . The velocity function reduced because Lorentz force resists the decline in flow speed at the surface.

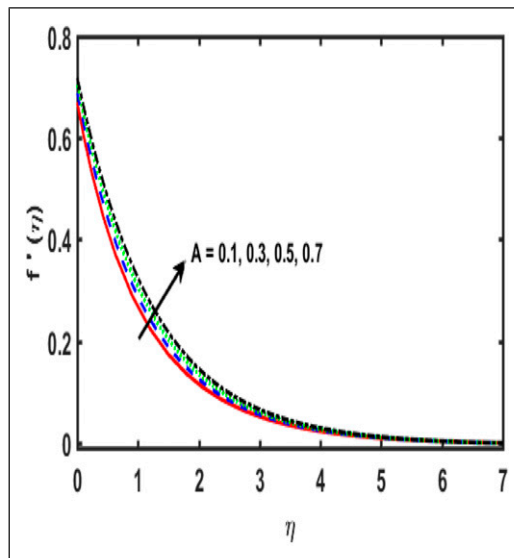


Figure 2. Variation of $f'(\eta)$ and A .

Figure 4 presents the variation of the magnetic profile $h'(\eta)$ and A . The magnetic profile is enhanced due to larger values of A . The thickness of the magnetic profile enhances with augmented values of the material parameter. The relation of P_{rm} and $h'(\eta)$ is revealed in Figure 5. Raising the values of P_{rm} which resist to increase the magnetic profile because thickness of the magnetic profile rised for higher values of P_{rm} . As the induced current density rises due to higher values of P_{rm} due to the effect of these phenomena, the induced magnetic profile thickness is enhanced. The relation of M and $h'(\eta)$ is revealed in Figure 6. Raising the values of M which resist to increase the magnetic profile because thickness of the magnetic profile rised for higher values of M . Figure 7 exposes the impacts of N_b on the temperature function $\theta(\eta)$. The thermal thickness is enhanced due to higher values of N_b . The Brownian motion parameter increases which enhances the temperature due to stronger molecular motion. Figure 8 depicted the impact of P_r on the temperature function $\theta(\eta)$. It is noted that thermal thickness reduced due to enhanced values of P_r . The thickness of the thermal boundary layer is reduced as the Prandtl number rises. The ratio of momentum diffusivity to heat diffusivity is known as the Prandtl number. P_r controls the relative thickening of the motion and heat flux zones in heat transfer problems. Figure 9 highlights the effects of S_1 on the temperature function. The temperature function is enhanced due higher values of S_1 because the thermal slip is enhanced which enhances the temperature function. The variation of N_t and $\varphi(\eta)$ is presented in Figure 10. The thickness of $\varphi(\eta)$ is enhanced because N_t increased. The distribution of concentrations becomes more non-uniform. Likewise, thermophoresis promotes non-uniformity in the concentration distribution, with a stronger effect at significantly greater concentrations. Figure 11 depicts the impacts of L_e on $\varphi(\eta)$. It is seen that thickness of $\varphi(\eta)$ is reduced due to higher values of L_e . Physically, the Lewis number is ratio of thermal and mass diffusivity. It is used to describe the flow of fluid in which heat and mass transfers occur simultaneously. The effects of N_b on $\varphi(\eta)$ are revealed in Figure 12. The thickness of concentration profile is enhanced due to enhanced values of N_b because of the movement of the particles from a higher concentration area to lower concentration area. Figure 13 depicts the effects of S_2 on $\varphi(\eta)$. It is noted that the higher values of S_2 resist the

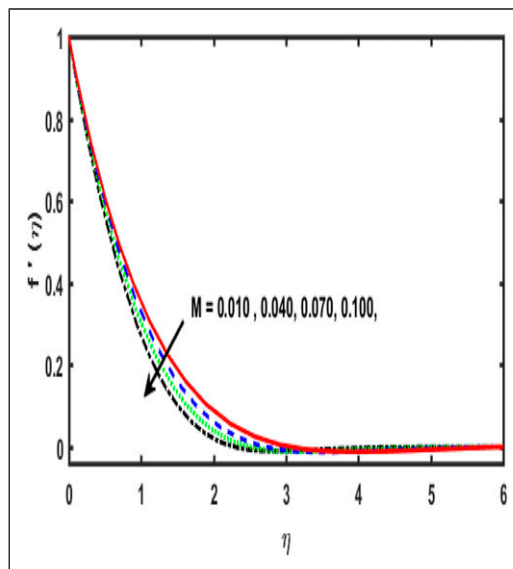


Figure 3. Variation of $f'(\eta)$ and M .

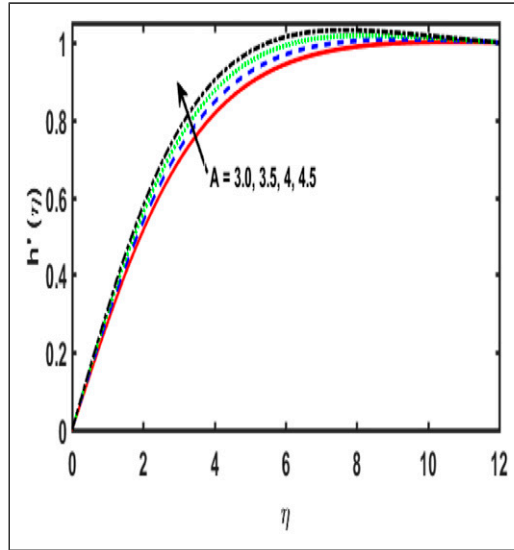


Figure 4. Variation of $h'(\eta)$ and A .

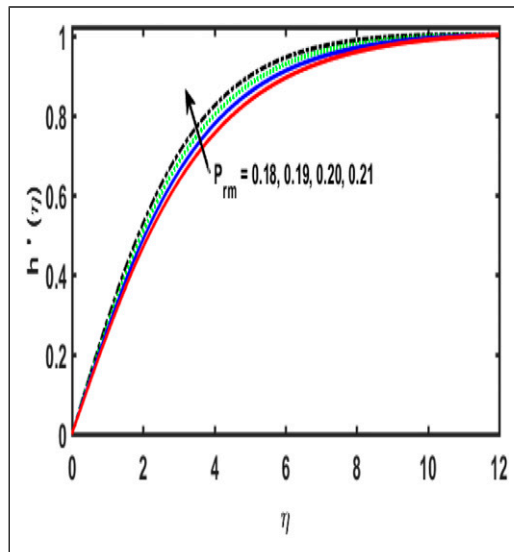


Figure 5. Variation of $h'(\eta)$ and P_{rm} .

enhancement of the values of the concentration profile. The concentration profile resisted due to slip of concentration enhances. Figure 14 presents the impacts of S_c on $\varphi(\eta)$. It is noted that the thickness of the concentration function is reduced due to higher values of S_c . Actually, S_c is directly proportional to the momentum diffusivity and inversely proportional to the mass diffusivity; consequently, the greater values of S_c conformed to the small mass diffusivity which caused decline in the concentration function. Figure 15 depicts the effects of τ_1 on $\varphi(\eta)$. The findings show that the

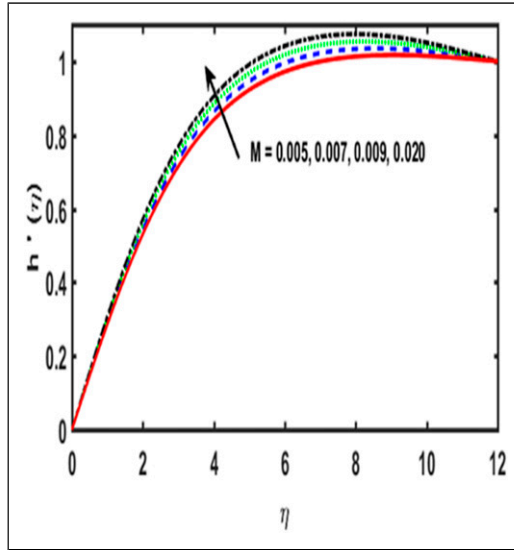


Figure 6. Variation of $h'(\eta)$ and M .

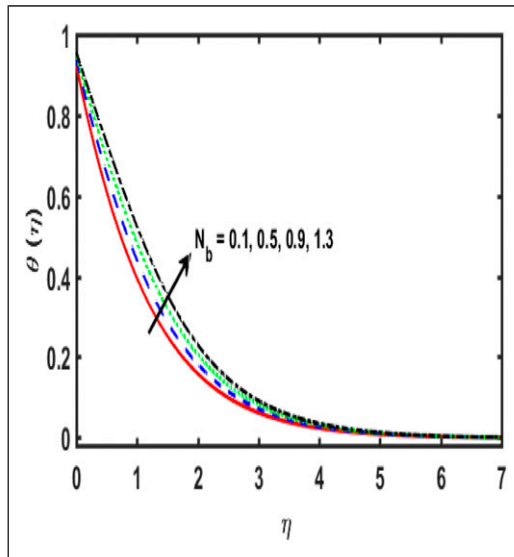


Figure 7. Variation of $\theta(\eta)$ and N_b

concentration distribution gets more non-uniform as the particle size increases which resists the reduction of the values of the concentration profile.

Tables 1–2 presented the effects of physical parameters on $f''(0)$, $-\theta'(\eta)$, and $-\phi'(0)$. The effects of material parameter A increased which reduces the skin friction. Because the viscosity of the fluid near the surface enhanced due to enhanced the material parameter which resist to reduce the skin

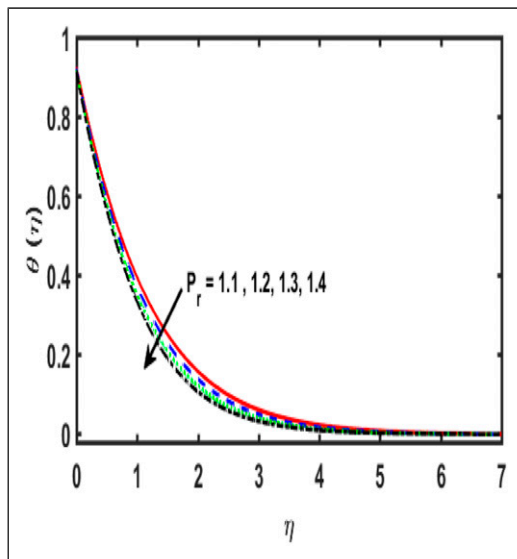


Figure 8. Variation of $\theta(\eta)$ and P_r

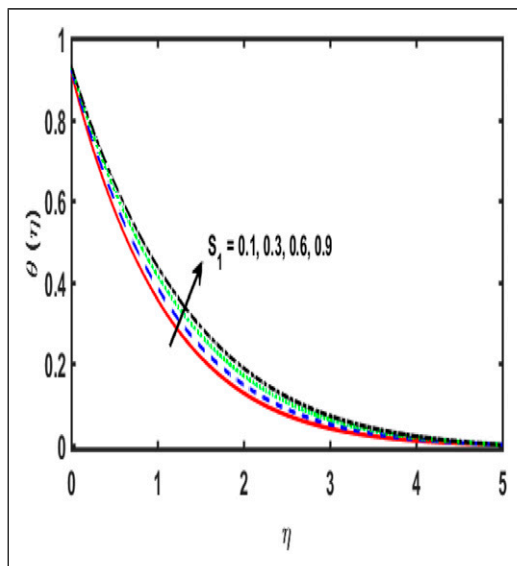


Figure 9. Variation of $\theta(\eta)$ and S_1

friction. The variation of the skin friction and magnetic field parameter is presented in [Table 1](#). The values of $f''(0)$ are enhanced due to higher values of M . These phenomena reduce the velocity profile because the thickness of the fluid is enhanced due to enhanced skin friction. The impacts of P_{rm} on $f''(0)$ are highlighted in [Table 1](#). It is observed that skin friction $f''(0)$ is enhanced for higher values of P_{rm} . It is noted that motion of the fluid reduced which reduces the skin friction due to

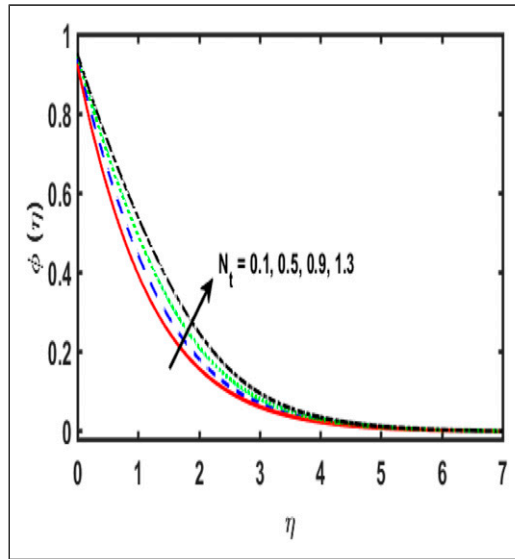


Figure 10. Variation of $\varphi(\eta)$ and N_t

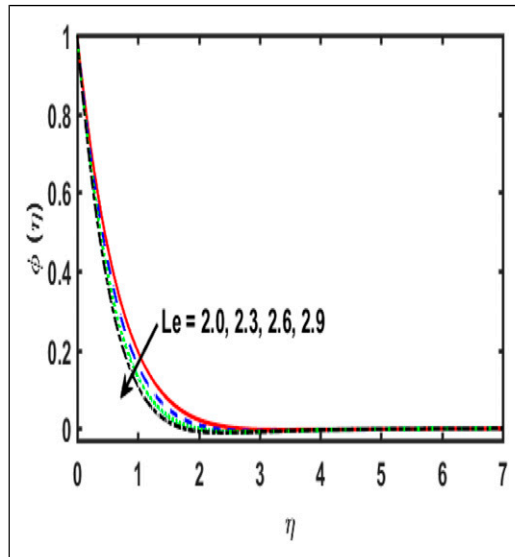


Figure 11. Variation of $\varphi(\eta)$ and Le

higher values of P_{rm} . The variation of E_c and $f''(0)$ is presented in Table 2. There is no variation found between E_c and $f''(0)$.

The variation of N_b and $-\theta'(\eta)$ and $-\varphi'(0)$ which reveals in Table 2. It is noted that values of $-\theta'(\eta)$ increase because Brownian motion parameter enhances, which improve the heat transfer rate because the movement of the particles of concentration is from higher area to lower area. The values

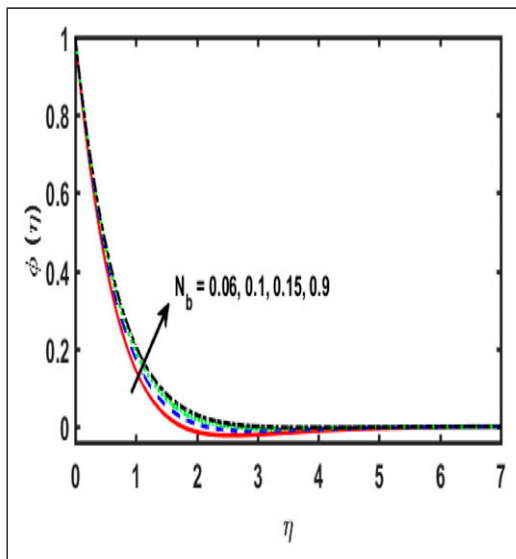


Figure 12. Variation of $\phi(\eta)$ and N_b

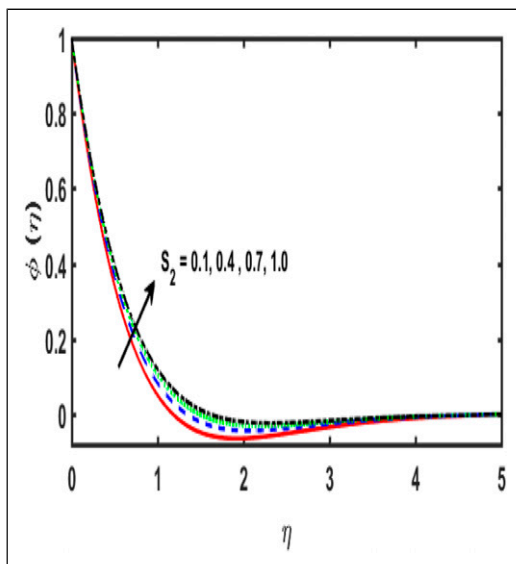


Figure 13. Variation of $\phi(\eta)$ and S_1

of $-\phi'(0)$ increased due to higher values of N_b , because the motion of the particle is enhanced which enhances $-\phi'(0)$. The $\phi(\eta)$ thickness enhances due to enhanced values of N_b because the movement of the particles of concentration is from higher area to lower area. The variation of the N_t and $-\theta'(\eta)$ and $-\phi'(0)$ which reveals in Table 2. It is noted that values of $-\theta'(\eta)$ increase with higher

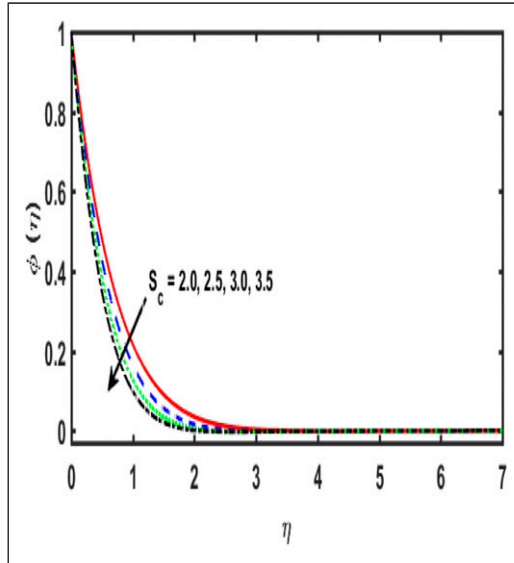


Figure 14. Variation of $\varphi(\eta)$ and S_c

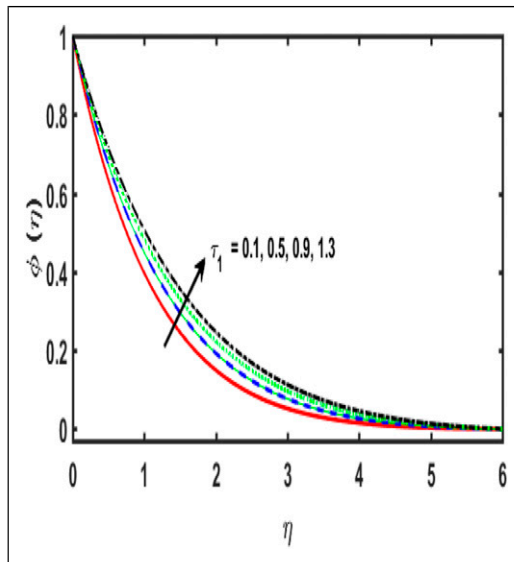


Figure 15. Variation of $\varphi(\eta)$ and τ_1

values of thermophoresis parameter which increase the heat transfer rate, while the values of $-\varphi'(0)$ decline due to higher values of N_t because the effect becomes more pronounced as the average concentration increases. The impacts of E_c on $-\theta'(\eta)$ and $-\varphi'(0)$ are presented in Table 2. It is noted that the values of Pr are enhanced which enhance the heat transfer rate at the contact point of the

Table 1: Skin friction against various parameters.

A	M	P_{rm}	E_c	$f''(0)$
0.1	0.3	0.3	1.2	1.27703
0.2	—	—	—	1.46242
0.3	—	—	—	1.63755
0.2	0.1	—	—	0.25489
—	0.2	—	—	0.24021
—	0.3	—	—	1.22848
—	—	0.1	—	1.24821
—	—	0.2	—	1.23683
—	—	0.3	—	1.21974
—	—	—	1.0	1.24821
—	—	—	1.5	1.24821
—	—	—	2.0	1.21821

Table 2: $-\theta'(0)$ and $-\phi'(0)$ against various parameters.

A	N_b	N_t	E_c	Pr	τ_1	S_c	$-\theta'(0)$	$-\phi'(0)$
0.1	—	—	—	—	—	—	1.00294	0.3483
0.2	—	—	—	—	—	—	1.00145	0.3541
0.3	—	—	—	—	—	—	0.999877	0.3594
0.3	0.1	—	—	—	—	—	1.00294	0.3483
—	0.2	—	—	—	—	—	1.00172	0.3015
—	0.3	—	—	—	—	—	1.0005	0.2859
—	—	0.0	—	—	—	—	1.00331	0.2556
—	—	0.5	—	—	—	—	0.98525	0.4014
—	—	0.6	—	—	—	—	0.981742	0.4289
—	—	—	0.3	—	—	—	0.246018	0.2891
—	—	—	0.5	—	—	—	0.253782	0.2923
—	—	—	0.7	—	—	—	0.261544	0.2956
—	—	—	—	0.1	—	—	0.238251	0.2859
—	—	—	—	0.2	—	—	0.330193	0.3186
—	—	—	—	0.3	—	—	0.41175	0.368
—	—	—	—	—	0.1	—	0.238251	0.2859
—	—	—	—	—	0.2	—	0.238257	0.2834
—	—	—	—	—	0.3	—	0.238263	0.2810
—	—	—	—	—	—	0.1	0.238251	0.2859
—	—	—	—	—	—	0.2	0.238129	0.3872
—	—	—	—	—	—	0.3	0.238033	0.4795

surface and fluid while the values of $-\phi'(0)$ increased. The heat transfer reduced due to higher values of Pr . The variation of τ_1 and $-\theta'(\eta)$ and $-\phi'(0)$ which reveals in Table 2. It is noted that values of the $-\theta'(\eta)$ increase, while the values of $-\phi'(0)$ decline due to higher values of τ_1 . The

variation of the S_c and $-\theta'(\eta)$ and $-\varphi'(0)$ which reveals in Table 2. It is noted that values of $-\theta'(\eta)$ increase, while the values of $-\varphi'(0)$ decline due to higher values of S_c .

Final remarks

We considered the two-dimensional flow of second-grade fluid under the induced magnetic field over an exponential stretching sheet. The variable thermal conductivity and viscous dissipation under the chemical reaction effects at exponentially stretching sheet are discussed in this analysis. The following achievements are highlighted:

- Velocity concentration profile is enhanced due to larger values of A but declines for higher values of M .
- Material parameter A and Prandtl number P_r are enhanced which resist the decrease in the temperature and concentration profiles.
- Magnetic profile is raised due to higher values of the material parameter A , P_{rm} , and M .
- $-\theta'(0)$ is enhanced for various values of A , but the inverse tendency of the Nusselt number is noticed for larger values of M and P_{rm} .
- $-\varphi'(0)$ increases by higher values of A , N_t , E_c , P_r , and τ_1 but declines for larger values of N_b and τ_1 .

Acknowledgment

The authors extend their appreciation to the Deanship of Scientific Research at King Khalid University for funding this work through research groups program under Grant No. R.G.P.1/183/42.

Declaration of conflicting interests

The author(s) declared no potential conflicts of interest with respect to the research, authorship, and/or publication of this article.

Funding

The author(s) disclosed receipt of the following financial support for the research, authorship, and/or publication of this article: This work was supported by the King Khalid University Grant No. R.G.P.1/183/42.

References

1. Damseh RA. Thermal boundary layer on an exponentially stretching continuous surface in the presence of magnetic field effect. *Int J Appl Mech Eng* 2006; 11(2): 289–299.
2. Ishak A. MHD boundary layer flow due to an exponential stretching sheet with radiation effect. *Sains Malays* 2011; 40(4): 391–395.
3. Elbashareshy EMA, Emam TG and Abdelgaber KM. Effects of thermal radiation and magnetic field on unsteady mixed convection flow and heat transfer over an exponentially stretching surface with suction in the presence of internal heat generation/absorption. *J Egypt Math Soc* 2012; 20(3): 215–222.
4. Nadeem S, Ul Haq R and Lee C. MHD flow of a Casson fluid over an exponentially shrinking sheet. *Sci Iran* 2012; 19(6): 1550–1553.
5. Ferdows M, Khan M, Alam M, et al. MHD mixed convective boundary layer flow of a nanofluid through a porous medium due to an exponentially stretching sheet. *Math Probl Eng*; 2012: 408528. DOI: [10.1155/2012/408528](https://doi.org/10.1155/2012/408528).

6. Hayat T, Khan MI, Waqas M, et al. Diffusion of chemically reactive species in third grade fluid flow over an exponentially stretching sheet considering magnetic field effects. *Chin J Chem Eng* 2017; 25(3): 257–263.
7. Khan AA, Naeem S, Ellahi R, et al. Dufour and sores effects on darcy-forchheimer flow of second-grade fluid with the variable magnetic field and thermal conductivity. *Int J Numer Methods Heat Fluid Flow* 2020; 30(9): 4331–4347.
8. Riaz MB, Saeed ST and Baleanu D. Role of magnetic field on the dynamical analysis of second grade fluid: an optimal solution subject to non-integer differentiable operators. *J Appl Comput Mech* 2020; 7(1): 54–68.
9. Hayat T, Khan WA, Abbas SZ, et al. Impact of induced magnetic field on second-grade nanofluid flow past a convectively heated stretching sheet. *Appl Nanosci* 2020; 10(8): 3001–3009.
10. Anwar T, Kumam P, Asifa I, et al. An exact analysis of radiative heat transfer and unsteady MHD convective flow of a second-grade fluid with ramped wall motion and temperature. *Heat Transfer* 2021; 50(1): 196–219.
11. Magyari E and Keller B. Heat and mass transfer in the boundary layers on an exponentially stretching continuous surface. *J Phys D: Appl Phys* 1999; 32(5): 577–585.
12. Partha M, Murthy P and Rajasekhar G. Effect of viscous dissipation on the mixed convection heat transfer from an exponentially stretching surface. *Heat Mass Transfer* 2005; 41(4): 360–366.
13. Pal D. Mixed convection heat transfer in the boundary layers on an exponentially stretching surface with magnetic field. *Appl Math Comput* 2010; 217(6): 2356–2369.
14. Mukhopadhyay S. Slip effects on MHD boundary layer flow over an exponentially stretching sheet with suction/blowing and thermal radiation. *Ain Shams Eng J* 2013; 4(3): 485–491.
15. Mukhopadhyay S. MHD boundary layer flow and heat transfer over an exponentially stretching sheet embedded in a thermally stratified medium. *Alexandria Eng J* 2013; 52(3): 259–265.
16. Hussain T, Shehzad SA, Hayat T, et al. Radiative hydromagnetic flow of Jeffrey nanofluid by an exponentially stretching sheet. *Plos One* 2014; 9(8): e103719.
17. Bég OA, Khan MS, Karim I, et al. Explicit numerical study of unsteady hydromagnetic mixed convective nanofluid flow from an exponentially stretching sheet in porous media. *Appl Nanosci* 2014; 4(8): 943–957.
18. Veerasha P, Prakasha DG and Kumar S. A fractional model for propagation of classical optical solitons by using nonsingular derivative. *Math Methods Appl Sci* 2020; 1–15. DOI: [10.1002/mma.6335](https://doi.org/10.1002/mma.6335).
19. Kumar S, Kumar R, Cattani C, et al. Chaotic behaviour of fractional predator-prey dynamical system. *Chaos, Solitons & Fractals* 2020; 135: 109811.
20. Kumar S, Ahmadian A, Kumar R, et al. An efficient numerical method for fractional SIR epidemic model of infectious disease by using Bernstein wavelets. *Mathematics* 2020; 8(4): 558.
21. Kumar S, Kumar R, Momani S, et al. A study on fractional COVID-19 disease model by using Hermite wavelets. *Math Methods Appl Sci* 2021. DOI: [10.1002/mma.7065](https://doi.org/10.1002/mma.7065).
22. Choi SU and Eastman JA. Enhancing Thermal Conductivity of Fluids with Nanoparticles (No. ANL/MSD/CP-84938. CONF-951135-29). IL (United States): Argonne National Lab., 1995.
23. Khan WA and Pop I. Boundary-layer flow of a nanofluid past a stretching sheet. *Int Journal Heat Mass Transfer* 2010; 53(11–12): 2477–2483.
24. Makinde OD and Aziz A. Boundary layer flow of a nanofluid past a stretching sheet with a convective boundary condition. *Int J Therm Sci* 2011; 50(7): 1326–1332.
25. Rana P and Bhargava R. Flow and heat transfer of a nanofluid over a nonlinearly stretching sheet: a numerical study. *Commun Nonlinear Sci Numer Simulation* 2012; 17(1): 212–226.
26. Hady FM, Ibrahim FS, Abdel-Gaied SM, et al. Radiation effect on viscous flow of a nanofluid and heat transfer over a nonlinearly stretching sheet. *Nanoscale Res Lett* 2012; 7(1): 229–313.

27. Rashidi MM, Vishnu Ganesh N, Abdul Hakeem AK, et al. Buoyancy effect on MHD flow of nanofluid over a stretching sheet in the presence of thermal radiation. *J Mol Liquids* 2014; 198: 234–238.
28. Gireesha BJ, Umeshaiyah M, Prasannakumara BC, et al. Impact of nonlinear thermal radiation on magnetohydrodynamic three dimensional boundary layer flow of Jeffrey nanofluid over a nonlinearly permeable stretching sheet. *Physica A: Stat Mech Its Appl* 2020; 549: 124051.
29. Ghanbari B, Kumar S and Kumar R. A study of behaviour for immune and tumor cells in immunogenetic tumour model with non-singular fractional derivative. *Chaos, Solitons & Fractals* 2020; 133: 109619.
30. Doungmo Goufo EF, Kumar S and Mugisha SB. Similarities in a fifth-order evolution equation with and with no singular kernel. *Chaos, Solitons & Fractals* 2020; 130: 109467.
31. Kumar S, Kumar R, Agarwal RP, et al. A study of fractional lotka-volterra population model using haar wavelet and adams-bashforth-moulton methods. *Math Methods Appl Sci* 2020; 43(8): 5564–5578.
32. Kumar S, Ghosh S, Samet B, et al. An analysis for heat equations arises in diffusion process using new yang-abdel-aty-cattani fractional operator. *Math Methods Appl Sci* 2020; 43(9): 6062–6080.
33. Kumar S, Chauhan RP, Momani S, et al. *Numerical Methods for Partial Differential Equations*, 2020, DOI: [10.1002/num.22707](https://doi.org/10.1002/num.22707).

Appendix

Notation

ρ	Density
ν	Kinematic viscosity
(u, v)	Velocity components
μ	Dynamic viscosity
(x, y)	Space coordinates
(H_1, H_2)	Components of induced magnetic field
P_r	Prandtl number
T	Temperature
C_p	Heat capacity
α_1	Material constant
$K(T)$	Thermal conductivity depending upon temperature
D_B	Brownian motion
C	Concentration of second-grade fluid
D_T	Thermophoresis
T_∞	Ambient temperature
K_∞	Thermal conductivity of the fluid
ε	Small parameter
U_0	Reference velocity
T_0	Ambient temperature
C_∞	Ambient concentration
C_0	Ambient estimation for concentration
η	Dimensionless variable
H_0	Ambient estimation for magnetic field
α	Second-grade nanofluid parameter
M	Magnetic field parameter
P_{rm}	Magnetic Prandtl number
N_b	Brownian motion parameter

L_e	Lewis number
τ_w	Wall shear stress
q_w	Wall heat flux
$\sqrt{Re} C_{fx}$	Dimensionless expression skin of friction
N_u	Dimensionless expression of the Nusselt number
Sh_x	Dimensionless expression of the Sherwood number
N_t	Thermophoresis parameter
θ	Temperature
φ	Concentration